

# Thermal Non-equilibrium Heat Transfer and Entropy Generation due to Natural Convection in a Cylindrical Enclosure with a Truncated Conical, Heat-Generating Porous Bed

Aranyak Chakravarty<sup>1,2</sup> · Priyanka Datta<sup>2</sup> · Koushik Ghosh<sup>2</sup> · Swarnendu Sen<sup>2</sup> · Achintya Mukhopadhyay<sup>2</sup>

Received: 13 April 2016 / Accepted: 3 October 2016 / Published online: 18 October 2016  
© Springer Science+Business Media Dordrecht 2016

**Abstract** Natural convection in enclosures driven by heat-generating porous media has diverse applications in fields like geothermal, chemical, thermal and nuclear energy. The present article focuses on heat transfer and entropy generation characteristics of a heat-generating porous bed, placed centrally within a fluid-filled cylindrical enclosure. Pressure drop and heat transfer in the porous bed are modelled using the Darcy–Brinkmann–Forschheimer approximation and the local thermal non-equilibrium model, respectively. Energy flux vectors have been utilised for visualising convective energy transfer within the enclosure. The study of a wide range of Rayleigh number ( $10^7$ – $10^{11}$ ) and Darcy number ( $10^{-6}$ – $10^{-10}$ ) reveals that heat transfer in the porous region can be classified into conduction-dominated and convection-dominated regimes. This is supplemented with an entropy generation analysis in order to identify and characterise the irreversibilities associated with the phenomenon. It is observed that entropy generation characteristics of the enclosure closely follow the above-mentioned regime demarcation. Numerical computations for the present study have been conducted using ANSYS FLUENT 14.5. The solid energy equation is solved as a user-defined scalar equation, while data related to energy flux vectors and entropy generation are obtained using user-defined functions.

**Keywords** Natural convection · Heat generation · Porous bed · Entropy generation · Thermal non-equilibrium

## List of Symbols

$a_i$	Interfacial area density ( $\text{m}^{-1}$ )
$Be$	Bejan number
$c_p$	Specific heat capacity ( $\text{J/kg K}$ )

✉ Koushik Ghosh  
kghosh@mech.jdvu.ac.in

<sup>1</sup> School of Nuclear Studies and Applications, Jadavpur University, Kolkata 700032, India

<sup>2</sup> Department of Mechanical Engineering, Jadavpur University, Kolkata 700032, India

$D_p$	Particle diameter (m)
$Da$	Darcy number
$E$	Dimensionless energy flux vector
$E_c$	Eckert number
$F_c$	Forchheimer coefficient
$g$	Acceleration due to gravity ( $m/s^2$ )
$h$	Heat transfer coefficient ( $W/m^2 K$ )
$H$	Bed height (m)
$k$	Thermal conductivity ( $W/m K$ )
$K$	Permeability ( $m^2$ )
$L$	Enclosure height (m)
$Nu$	Nusselt number
$NS'''$	Dimensionless volumetric entropy generation rate
$P$	Pressure (Pa)
$Pr$	Prandtl number
$q'''$	Volumetric heat generation rate ( $W/m^3$ )
$q_i$	Heat flux at fluid–porous interface
$r, z$	Cylindrical co-ordinates (m)
$R$	Bed radius (m)
$Ra$	Rayleigh number
$Re$	Reynolds' number
$T$	Temperature (K)
$U, V$	Velocity ( $ms^{-1}$ )

## Greek Letters

$\alpha$	Thermal diffusivity ( $m^2/s$ )
$\beta$	Thermal expansion coefficient ( $1/K$ )
$\gamma$	Porosity-scaled thermal conductivity ratio
$\varepsilon$	Porosity
$\phi$	Bed angle ( $^\circ$ )
$\mu$	Dynamic viscosity ( $kg/ms$ )
$\nu$	Kinematic viscosity ( $m^2/s$ )
$\theta$	Dimensionless temperature
$\rho$	Density ( $kg/m^3$ )
$\psi$	Sphericity of solid particles
$ \psi $	Dimensionless absolute stream function
$\Pi$	Dimensionless heat function
$\Phi$	Dissipation function

## Subscripts

avg	Average value
c	Cold wall of the enclosure
f	Fluid phase
max	Maximum value
p	Porous medium
s	Solid phase
sf	Solid to fluid phase of porous medium
wall	Enclosure wall

## Superscript

/ Dimensionless quantities

### 1 Introduction

Natural convection in porous media driven by internal heating is an important phenomenon occurring in several natural as well as industrial processes. These include convection within the earth's mantle (Mckenzie et al. 1974), extraction of geothermal energy (Glassley 1995), cooling of material stockpiles (Ejlali and Hooman 2011), post-accident heat removal from nuclear debris beds (Takasuo et al. 2012), disposal of radioactive wastes in underground repositories (Toth 2011) etc. Of late, this phenomenon has been receiving considerable attention due to its relevance mainly in nuclear safety applications. Absence or inadequate cooling of a nuclear reactor core may cause melting of the core and subsequently result in the formation of a heat-generating porous debris bed within the reactor pressure vessel due to molten fuel-coolant interactions. The natural shape of such porous debris beds is a conical heap (Takasuo et al. 2012; Chakravarty et al. 2016). Stockpiles of self-igniting material as coal are also of a similar shape (Ejlali and Hooman 2011). The major concern in the above-mentioned situations is to limit the temperature rise to acceptable levels for ensuring system safety. As such, it is of considerable interest to predict the convectational fluid flow and temperature distribution for optimal design of such systems.

Precise prediction of thermal performance of a system is essential for ensuring system safety in the above-stated applications. Literature review shows that the local thermal equilibrium (LTE) model of energy transfer in porous media, which assumes that the saturating fluid and the constituent solid particles are at the same temperature, is usually followed for analysing natural convective heat transfer involving porous media. However, this approximation is known to induce substantial error in case of certain applications, such as the problem under consideration in the present study (Minkowycz et al. 1999; Bortolozzi and Deiber 2001; Rees and Pop 2005; Nield and Bejan 2006), and this necessitates the use of the local thermal non-equilibrium (LTNE) model of the energy equation. In the LTNE model, a finite temperature difference is assumed between the solid and the fluid phases leading to heat transfer between the two phases. Thus, a more accurate modelling of thermal conditions in a porous system is possible using the LTNE approach (Baytaş 2003). This concept has been utilised in modelling various natural as well as forced convection problems (Alazmi and Vafai 2002; Baytaş and Pop 2002; Nield et al. 2002).

Although several works have been carried out on natural convection involving heat-generating porous media using the LTE model (Prasad 1987; Jue 2003; Chakravarty et al. 2016), only a limited number of studies are available on heat-generating porous media using the LTNE approach. Baytaş (2003) modelled steady natural convection in a heat-generating porous square enclosure, bounded with isothermal cold walls utilising the LTNE approach. It was established that for a given  $Ra$ ,  $Da$  and  $Pr$ , the assumption of LTE is valid for large values of the dimensionless heat transfer coefficient between solid and fluid phases and porosity-scaled thermal conductivity ratio, while at smaller values the use of LTNE is indispensable. Nouri-Borujerdi et al. (2007b) and Saravanan (2009) carried out linear stability analyses to determine the onset of natural convection in fluid-saturated porous medium with uniform heat generation using the LTNE model. Nouri-Borujerdi et al. (2007a) also studied the effect of LTNE on conduction in a heat-generating porous layer and determined the exact

solutions of temperature profiles within the channel. Saravanan and Senthil Nayaki (2014) studied convective instability in a horizontal heat-generating porous layer, with temperature-dependent fluid viscosity, and heated from below. Kuznetsov and Nield (2014) analytically studied the effect of local thermal non-equilibrium on the onset of convection in a porous medium consisting of two internally heated horizontal layers. A similar study by Kuznetsov and Nield (2015) focussed on internally heated horizontal porous layers with vertical through-flow. Mahmoudi (2015) analytically investigated forced convection in a micro-channel filled with heat-generating porous material saturated with rarefied gas under constant heat flux boundary condition. Wu et al. (2015a) carried out a numerical study of steady non-Darcy natural convection in a square enclosure with partially cooled walls and filled with heat-generating porous medium. Analysis of different cooling configurations with both LTE and LTNE models showed that a higher local Nusselt number is achieved in the partial cooling configuration as compared to a fully cooled wall. A similar study by Wu et al. (2015b) with adiabatic horizontal walls and sinusoidal temperature distribution on the side walls showed heat transfer enhancement as compared to a uniform temperature distribution.

In addition to accurate modelling of the thermal performance, an important requirement for the safe operation of such critical systems is to ensure sufficient heat transfer from the enclosure. One such route of ensuring sufficient heat transfer is through the reduction of associated irreversibilities or minimisation of entropy generation within a system, the basics of which has been detailed by Bejan (1996). This method focuses on identification of mechanisms or system components that contribute to thermodynamic losses, determination of the magnitude of such losses or irreversibilities (which lead to entropy generation) and subsequently its minimisation, such that the overall thermodynamic efficiency could be improved. This technique has been successfully applied to a wide range of thermal systems involving natural convection in different geometrical configurations and composed of pure fluid as well as porous materials (Famouri and Hooman 2008; Mukhopadhyay 2010; Kaluri and Basak 2011; Datta et al. 2016). A pertinent work in the present context is that by Baytaş (2007) which reported an entropy generation analysis considering heat-generating porous media using the LTNE approach.

In all the above cited studies on natural convection considering heat-generating porous media using the LTNE approach, geometries have been considered to be fully filled with porous media. In view of the stated applications, however, it is more probable that such geometries may not be fully filled with porous materials. Literature survey reveals that several studies are available on natural convection in partially-porous geometries with internal heat generation using the LTE approach (Schulenberg and Muller 1984; Du and Bilgen 1990; Chen and Lin 1997; Kim et al. 2001; Chakravarty et al. 2016). Schulenberg and Muller (1984) numerically modelled turbulent natural convection in a heat-generating porous layer with very low permeability and superposed by a clear fluid layer and developed a 1-D asymptotic correlation for Nusselt number. Du and Bilgen (1990) found that in addition to  $Ra$  and  $Da$ , heat transfer within a cavity is also affected by the position of the porous layer, aspect ratio, filling factor as well as cooling asymmetry from the side walls. Chen and Lin (1997) obtained multiple steady-state solutions with different flow patterns in an inclined porous layer and heat transfer performance was found to be affected by the tilt angle as well as aspect ratio of the enclosure. Chakravarty et al. (2016) observed that geometry of the porous zone significantly affects fluid flow and heat transfer in a cylindrical enclosure partially filled with a heat-generating truncated conical porous bed. In contrast, there is a dearth of such studies using the LTNE approach. In addition, a significant number of studies exist on entropy generation analysis in partial porous configurations (Torabi et al. 2015a, b), but none involving natural convection in heat-generating porous media with the use of the LTNE approach.

In a nutshell, the present study focuses on the thermal aspects of natural convection induced by a heat-generating porous bed within a cylindrical enclosure. The shape of the porous bed is assumed to be a truncated cone in order to approximate the heap-like structure of coal stockpiles (Ejlali and Hooman 2011) or corium debris beds formed as a consequence of severe accident in nuclear reactors (Takasuo et al. 2012). Adoption of this geometry is yet another novelty along with the LTNE approach used in this study. The analysis is carried out, and the results are presented in a dimensionless form in terms of Rayleigh number, Darcy number, stream function, isotherms, energy flux vectors and Nusselt number. This is supplemented by an entropy generation analysis to determine the effect of various pertinent parameters on system irreversibility. The entire study has been performed using the computational fluid dynamics software ANSYS FLUENT 14.5. The solid energy equation within the porous bed is solved with the help of user-defined scalar (UDS) equation utility, while data related to energy flux vectors and entropy generation are obtained using user-defined functions (UDF) in ANSYS FLUENT.

## 2 Problem Statement

A schematic representation of the problem under consideration is shown in Fig. 1. A fluid-filled cylindrical enclosure contains a centrally located material bed composed of fluid-saturated porous media. Heat generation is assumed within the solid particles constituting the porous bed. All walls of the enclosure are impermeable, with the top and side wall isothermally cooled and the bottom wall adiabatic. The porous bed is modelled as a truncated cone which approximates the general shape of a material debris bed such as a coal stockpile or a corium debris bed formed subsequent to a severe accident in a nuclear reactor (Chakravarty et al. 2016). The entire geometry is axisymmetric about the  $z$  axis.

It is assumed that the porous medium is homogeneous and isotropic, and the constituent solid particles are perfectly spherical. Flow through the porous bed is approximated using the Darcy–Brinkmann–Forchheimer model. Furthermore, it is assumed that the saturating fluid and the solid particles in the porous bed are not in local thermal equilibrium and hence, energy transfer takes place between the heat-generating solid phase and the saturating fluid. Fluid flow is single phase and laminar. In addition, the fluid is assumed to be Newtonian and satisfies the Boussinesq approximation.

### 2.1 Governing Equations

Under the above-stated assumptions, the dimensionless form of the steady-state, two-dimensional governing equations for the clear fluid region can be written in the following form

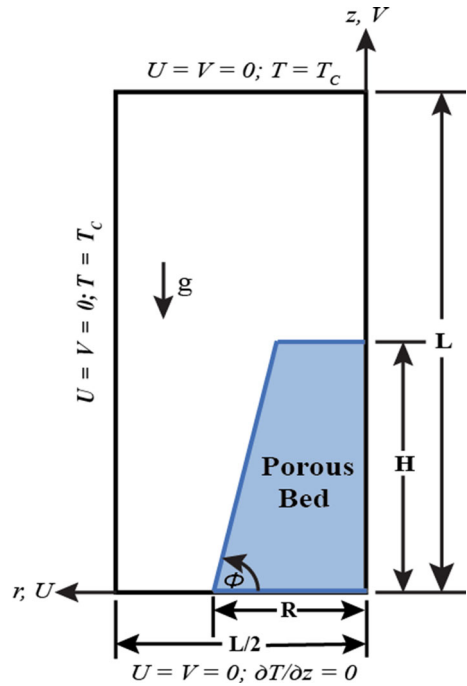
*Mass Balance :*

$$\frac{1}{r'} \frac{\partial(r'U')}{\partial r'} + \frac{\partial V'}{\partial z'} = 0, \quad (1)$$

*Momentum Balance:*

$$\left( U' \frac{\partial U'}{\partial r'} + V' \frac{\partial U'}{\partial z'} \right) = - \frac{\partial P'}{\partial r'} + Pr \left( \frac{1}{r'} \frac{\partial}{\partial r'} \left( r' \frac{\partial U'}{\partial r'} \right) - \frac{U'}{r'^2} + \frac{\partial^2 U'}{\partial z'^2} \right), \quad (2)$$

**Fig. 1** Schematic representation of the problem geometry



$$\left( U' \frac{\partial V'}{\partial r'} + V' \frac{\partial V'}{\partial z'} \right) = - \frac{\partial P'}{\partial z'} + Pr \left( \frac{1}{r'} \frac{\partial}{\partial r'} \left( r' \frac{\partial V'}{\partial r'} \right) + \frac{\partial^2 V'}{\partial z'^2} \right) + \frac{RaPr}{H'^3} \theta_f, \quad (3)$$

Heat transport:

$$U' \frac{\partial \theta_f}{\partial r'} + V' \frac{\partial \theta_f}{\partial z'} = \left( \frac{1}{r'} \frac{\partial}{\partial r'} \left( r' \frac{\partial \theta_f}{\partial r'} \right) + \frac{\partial^2 \theta_f}{\partial z'^2} \right). \quad (4)$$

In a similar manner, the dimensionless form of the governing equations for the porous region following the Darcy–Brinkmann–Forchheimer model and the local thermal non-equilibrium (LTNE) approximation is written as

Mass Balance :

$$\frac{1}{r'} \frac{\partial (r' U')}{\partial r'} + \frac{\partial V'}{\partial z'} = 0, \quad (5)$$

Momentum Balance:

$$\begin{aligned} \frac{1}{\varepsilon^2} \left( U' \frac{\partial U'}{\partial r'} + V' \frac{\partial U'}{\partial z'} \right) &= - \frac{\partial P}{\partial r'} + \frac{Pr}{\varepsilon} \left( \frac{1}{r'} \frac{\partial}{\partial r'} \left( r' \frac{\partial U'}{\partial r'} \right) - \frac{U'}{r'^2} + \frac{\partial^2 U'}{\partial z'^2} \right) \\ &\quad - \frac{Pr}{Da H'^2} U' - \frac{F_c \sqrt{U'^2 + V'^2}}{\sqrt{Da} H' \varepsilon^{3/2}} U', \end{aligned} \quad (6)$$

$$\begin{aligned} \frac{1}{\varepsilon^2} \left( U' \frac{\partial V'}{\partial r'} + V' \frac{\partial V'}{\partial z'} \right) &= - \frac{\partial P'}{\partial z'} + \frac{Pr}{\varepsilon} \left( \frac{1}{r'} \frac{\partial}{\partial r'} \left( r' \frac{\partial V'}{\partial r'} \right) + \frac{\partial^2 V'}{\partial z'^2} \right) - \frac{Pr}{Da H'^2} V' \\ &\quad - \frac{F_c \sqrt{U'^2 + V'^2}}{\sqrt{Da} H' \varepsilon^{3/2}} V' + \frac{RaPr}{H'^3} \theta, \end{aligned} \quad (7)$$

Heat transport in fluid phase:

$$U' \frac{\partial \theta_f}{\partial r'} + V' \frac{\partial \theta_f}{\partial z'} = \left( \frac{1}{r'} \frac{\partial}{\partial r'} \left( r' \frac{\partial \theta_f}{\partial r'} \right) + \frac{\partial^2 \theta_f}{\partial z'^2} \right) + h' (\theta_s - \theta_f), \quad (8)$$

Heat transport in solid phase:

$$0 = \left( \frac{1}{r'} \frac{\partial}{\partial r'} \left( r' \frac{\partial \theta_s}{\partial r'} \right) + \frac{\partial^2 \theta_s}{\partial z'^2} \right) + \gamma \cdot h' (\theta_f - \theta_s) + \frac{2}{H'^2}. \quad (9)$$

The above equations are derived using the following dimensionless variables

$$\begin{aligned} r' &= \frac{r}{L}, \quad z' = \frac{z}{L}, \quad H' = \frac{H}{L}, \quad R' = \frac{R}{L}, \quad \alpha = \frac{k_f}{(\rho c_p)_f}, \quad U' = \frac{UL}{\alpha}, \quad V' = \frac{VL}{\alpha}, \quad P' = \frac{PL^2}{\rho \alpha^2}, \\ \theta &= \frac{T - T_c}{\Delta T_{\text{ref}}}, \quad \Delta T_{\text{ref}} = \frac{q''' H^2}{2k_s}, \quad Pr = \frac{\nu}{\alpha}, \quad Da = \frac{K}{H^2}, \quad Ra = \frac{g\beta \Delta T_{\text{ref}} H^3}{\nu \alpha}, \\ h' &= \frac{ha_i L^2}{\varepsilon k_f}, \quad \gamma = \frac{\varepsilon k_f}{(1 - \varepsilon) k_s}. \end{aligned}$$

In case of a packed porous bed composed of uniformly distributed spherical particles of same size, the permeability ( $K$ ) and the Forchheimer coefficient ( $F_c$ ) are expressed as

$$K = \frac{\psi^2 D_p^2 \varepsilon^3}{150 (1 - \varepsilon)^2} \quad \text{and} \quad F_c = \frac{1.75}{\sqrt{150}}. \quad (10)$$

In the above expression of permeability,  $\psi$  represents the shape factor or sphericity of the particles and is defined as the ratio between area of the equivalent-volume sphere and surface area of the particle. Since surface area of a perfectly spherical particle is equal to the area of an equivalent sphere, sphericity becomes unity and as such, in the present study  $\psi$  is assumed to be unity.

The assumption of local thermal non-equilibrium between the solid particles and the fluid medium saturating the porous bed necessitates the use of a heat transfer correlation between the solid and fluid phases. [Rees and Pop \(2005\)](#) summarises various heat transfer correlations that have been used over the years in evaluating solid to fluid heat transfer in porous media. Some of these correlations take into account the effect of solid thermal conductivity ([Dixon and Cresswell 1979](#)) while others, such as that reported by [Wakao et al. \(1979\)](#), do not explicitly consider solid thermal conductivity. [Alazmi and Vafai \(2000\)](#) analysed the variances among the different correlations with respect to various parameters, including the solid to fluid thermal conductivity ratio ( $k_s/k_f$ ), and concluded that solid thermal conductivity has a significant impact on interfacial heat transfer only at a very high thermal conductivity ratio ( $k_s/k_f \sim O(50)$ ). In the present study, the magnitudes of thermal conductivity assumed for the solid ( $k_s = 2.0$  W/mK) and fluid phases ( $k_f = 0.61057$  W/mK) of the porous bed result in a thermal conductivity ratio of 3.275. As such, it can be inferred that solid thermal conductivity will not have any substantial impact on the interfacial heat transfer. This also justifies the use of a heat transfer correlation which does not explicitly consider solid thermal conductivity.

The [Ranz and Marshall \(1952\)](#) model is a standard correlation generally used for flow over spherical particles ([Mahapatra et al. 2013](#)). Although it does not have explicit consideration of solid thermal conductivity, it has been extensively used in numerical modelling of situations involving porous media ([Kakaç et al. 1991](#)) and especially in case of nuclear debris beds ([Takasuo 2015](#)). As such, in the present study, the interfacial heat transfer coefficient ( $h$ )

between the solid particles and the fluid saturating the porous medium is evaluated using the correlation of [Ranz and Marshall \(1952\)](#). This is expressed in this work as

$$h = \frac{Nu_{sf}k_f}{D_p} = \frac{(2 + 0.66Re^{1/2}Pr^{1/3})k_f}{D_p}, \tag{11}$$

where the suffix *sf* represents heat transfer from the solid particles to the saturating fluid. Reynolds number (*Re*) used in Eq. (11) is calculated based on the intrinsic velocity  $U^*$  ( $U^* = U/\varepsilon$ ) in the porous bed and expressed as

$$Re = \frac{\rho_f D_p |U^*|}{\mu_f}. \tag{12}$$

The interfacial area density is defined as:

$$a_i = \frac{6(1 - \varepsilon)}{D_p}. \tag{13}$$

Heat transfer at the enclosure walls is estimated in terms of Nusselt number at the isothermal walls ( $Nu_{wall}$ ). This is expressed as follows, with *n* denoting the radial or axial directions

$$Nu_{wall} = -\frac{\partial\theta_f}{\partial n} \quad \text{and} \quad Nu_{wall, avg} = \frac{\int_0^1 Nu_{wall} dn}{\int_0^1 dn}. \tag{14}$$

The dimensionless forms of the boundary conditions are stated as

$$\begin{aligned} U' = V' = 0, \quad \theta_f = \theta_s = 0 \quad \text{at } r' = 0.5, 0 \leq z' \leq 1.0, \\ U' = V' = 0, \quad \theta_f = \theta_s = 0y \quad \text{at } z' = 1.0, 0 \leq r' \leq 0.5, \\ U' = V' = 0, \quad \frac{\partial\theta_f}{\partial z'} = \frac{\partial\theta_f}{\partial z'} = 0 \quad \text{at } z' = 0, 0 \leq r' \leq 0.5. \end{aligned} \tag{15}$$

The clear fluid region and the porous bed are modelled by creating two distinct cell zones in ANSYS Fluent. Interfaces of the two cell zones serve as the boundary between the porous bed and the fluid region. The dimensionless form of the fluid–porous interface conditions is expressed as

*Fluid flow condition:*

$$\begin{aligned} U'|_f = U'|_p \quad \text{and} \quad Pr \left( \frac{1}{r'} \frac{\partial}{\partial r'} \left( r' \frac{\partial U'}{\partial r'} \right) - \frac{U'}{r'^2} + \frac{\partial^2 U'}{\partial z'^2} \right) \Big|_f = \frac{Pr}{\varepsilon} \left( \frac{1}{r'} \frac{\partial}{\partial r'} \left( r' \frac{\partial U'}{\partial r'} \right) - \frac{U'}{r'^2} + \frac{\partial^2 U'}{\partial z'^2} \right) \Big|_p, \\ V'|_f = V'|_p \quad \text{and} \quad Pr \left( \frac{1}{r'} \frac{\partial}{\partial r'} \left( r' \frac{\partial V'}{\partial r'} \right) + \frac{\partial^2 V'}{\partial z'^2} \right) \Big|_f = \frac{Pr}{\varepsilon} \left( \frac{1}{r'} \frac{\partial}{\partial r'} \left( r' \frac{\partial V'}{\partial r'} \right) + \frac{\partial^2 V'}{\partial z'^2} \right) \Big|_p, \end{aligned} \tag{16}$$

*Heat transfer condition:*

$$\begin{aligned} \theta_f|_f = \theta_f|_p, \\ \nabla \cdot (\nabla\theta_f)|_f = q_i, \\ \nabla \cdot (\nabla\theta_f)|_p = \varepsilon q_i, \\ \nabla \cdot (\nabla\theta_s)|_p = (1 - \varepsilon)q_i. \end{aligned} \tag{17}$$



### 2.2 Energy Flux Vectors

In convective heat transfer processes, streamlines and isotherms are the most frequently used tools for visualisation and analysis of fluid flow and heat transfer. However, isotherms do not yield adequate information regarding the direction and magnitude of heat transfer. In this respect, the concept of heatlines and heatfunction was introduced by [Kimura and Bejan \(1983\)](#) for proper visualisation and analysis of heat transfer. Heatfunction takes into account the simultaneous transfer of energy by conduction and convection and as such, presents a comprehensive picture of energy transfer in a medium. However, it is not possible to define heat function in transient problems or for systems involving source terms due to the lack of a closed form solution. This shortcoming has been addressed by [Hooman \(2010\)](#) with the development of energy flux vectors. Since the present problem involves internal heat generation, the concept of energy flux vectors has been used for visualisation of convective energy transfer within the system. Mathematically, the energy flux vector can be expressed as

$$\vec{E} = \left(\frac{\partial \Pi}{\partial z'}\right) \vec{i} - \left(\frac{1}{r'} \frac{\partial \Pi}{\partial r'}\right) \vec{j}. \tag{18}$$

Following [Ejlali and Hooman \(2011\)](#) and [Ejlali et al. \(2009\)](#), the dimensionless form of energy flux vectors is separately defined for the fluid and porous regions as follows

*Fluid region:*

$$\frac{\partial \Pi}{\partial z'} = U' \theta_f - r' \frac{\partial \theta_f}{\partial r'}, \tag{19}$$

$$-\frac{1}{r'} \frac{\partial \Pi}{\partial r'} = V' \theta_f - \frac{\partial \theta_f}{\partial z'}, \tag{20}$$

*Porous region:*

$$\frac{\partial \Pi}{\partial z'} = U' \theta_f - r' \frac{\partial \theta_f}{\partial r'} - r' \frac{\partial \theta_s}{\partial r'} - \left[ (1 - \gamma) \frac{h'}{4} (\theta_s - \theta_f) r'^2 \right] - \frac{r'^2}{2H^2}, \tag{21}$$

$$-\frac{1}{r'} \frac{\partial \Pi}{\partial r'} = V' \theta_f - \frac{\partial \theta_f}{\partial z'} - \frac{\partial \theta_s}{\partial z'} - \left[ (1 - \gamma) \frac{h'}{2} (\theta_s - \theta_f) z' \right] - \frac{z'}{H^2}. \tag{22}$$

### 2.3 Entropy Generation

A literature survey reveals inconsistencies related to solid-fluid heat transfer and heat generation in entropy generation formulation for heat-generating porous media ([Baytaş 2007](#); [Betchen and Straatman 2008](#); [Ting et al. 2015](#); [Torabi et al. 2015a](#)). In order to resolve this, the local volumetric entropy generation rates for the present system have been derived using volume-averaging technique as detailed in [Faghri and Zhang \(2006\)](#). These are expressed separately for the fluid region as well as the solid and the fluid phases of the porous medium in a dimensionless form as follows

*Fluid region:*

$$\begin{aligned} NS_f''' &= NS_{f,\theta}''' + NS_{f,\psi}''' \\ &= \frac{1}{(\theta_f + T^*)} \left( \left( \frac{\partial \theta_f}{\partial z'} \right)^2 + \left( \frac{\partial \theta_f}{\partial r'} \right)^2 \right) + \frac{EcPr}{(\theta_f + T^*)} \Phi, \end{aligned} \tag{23}$$

Porous region:

$$\begin{aligned}
 NS'''_{pf} &= NS'''_{pf,\theta} + NS'''_{pf,\psi} + NS'''_{pf,Da} + NS'''_{pf,\theta fs} \\
 &= \frac{1}{(\theta_f + T^*)} \left( \left( \frac{\partial \theta_f}{\partial z'} \right)^2 + \left( \frac{\partial \theta_f}{\partial r'} \right)^2 \right) + \frac{EcPr}{(\theta_f + T^*)} \Phi + \frac{EcPr}{(\theta_f + T^*) Da} (U'^2 + V'^2) \\
 &\quad + \frac{h'(\theta_s - \theta_f)^2}{(\theta_f + T^*)(\theta_s + T^*)}, \tag{24}
 \end{aligned}$$

$$\begin{aligned}
 NS'''_{ps} &= NS'''_{ps,\theta} \\
 &= \frac{1}{(\theta_s + T^*)} \left( \left( \frac{\partial \theta_s}{\partial z'} \right)^2 + \left( \frac{\partial \theta_s}{\partial r'} \right)^2 \right). \tag{25}
 \end{aligned}$$

The quantity  $\Phi$  represents the dissipation function and is expressed for a two-dimensional, cylindrical coordinate system as

$$\Phi = 2 \left[ \left( \frac{\partial U'}{\partial r'} \right)^2 + \left( \frac{\partial V'}{\partial z'} \right)^2 + \left( \frac{U'}{r'} \right)^2 \right] + \left( \frac{\partial U'}{\partial z'} + \frac{\partial V'}{\partial r'} \right)^2. \tag{26}$$

The first two terms in Eqs. (23–24) represent irreversibility associated with heat transfer ( $NS'''_{f,\theta}$ ,  $NS'''_{pf,\theta}$ ) and viscous effect of fluid flow ( $NS'''_{f,\psi}$ ,  $NS'''_{pf,\psi}$ ), respectively. In Eq. (24), the third term is due to irreversibility caused by viscous drag in porous media ( $NS'''_{pf,Da}$ ), while the last term is associated with local heat transfer between the fluid and solid phases ( $NS'''_{pf,\theta fs}$ ). Form drag in porous media has negligible effects on entropy generation (Baytaş 2007) and has been neglected in the current study. Similarly, Eq. (25) represents irreversibility caused by heat transfer in the solid phase ( $NS'''_{ps,\theta}$ ). The total irreversibility due to heat transfer ( $NS'''_{\theta}$ ), fluid friction ( $NS'''_{\psi}$ ), viscous drag ( $NS'''_{Da}$ ), heat transfer between solid and fluid phases ( $NS'''_{\theta fs}$ ) and total entropy generation ( $NS'''$ ) is expressed as follows, where  $\Omega$  and  $\Lambda$  represent the clear fluid and porous domains, respectively,

$$NS'''_{\theta} = \int_{\Omega} NS'''_{f,\theta} d\Omega + \int_{\Lambda} (NS'''_{pf,\theta} + NS'''_{ps,\theta}) d\Lambda, \tag{27}$$

$$NS'''_{\psi} = \int_{\Omega} NS'''_{f,\psi} d\Omega + \int_{\Lambda} NS'''_{pf,\psi} d\Lambda, \tag{28}$$

$$NS'''_{Da} = \int_{\Lambda} NS'''_{pf,Da} d\Lambda, \tag{29}$$

$$NS'''_{\theta fs} = \int_{\Lambda} NS'''_{pf,\theta fs} d\Lambda, \tag{30}$$

$$NS''' = NS'''_{\theta} + NS'''_{\psi} + NS'''_{Da} + NS'''_{\theta fs}. \tag{31}$$

Equations (23–25) introduce two additional dimensionless quantities— $Ec$  and  $T^*$ —which are expressed as

$$Ec = \frac{\alpha^2}{L^2 C_p \Delta T_{ref}} = \frac{g\beta H^3}{L^2 C_p RaPr}, \tag{32}$$

$$T^* = \frac{T_c}{\Delta T_{ref}}. \tag{33}$$

In order to assess the dominance of entropy generation due to heat transfer irreversibility, with respect to that of fluid friction irreversibility and vice-versa, the average Bejan number ( $Be$ ) is defined as the ratio of entropy generation due to heat transfer irreversibility to the total entropy generation. Mathematically, it is expressed as

$$Be = \frac{NS''_{\theta} + NS''_{\theta_{fs}}}{NS''}. \quad (34)$$

It is worth mentioning here that  $Be > 0.5$  represents dominance of heat transfer irreversibility, while  $Be < 0.5$  represents dominance of fluid friction irreversibility.  $Be = 0.5$  indicates equal contribution from heat transfer irreversibility and fluid friction irreversibility towards total entropy generation.

### 3 Numerical Procedure

Numerical solution of the governing equations, Eqs. (1–9), is obtained following a control volume approach using the computational fluid dynamics software ANSYS FLUENT 14.5. PRESTO (PRESSure STaggering Option) is used as the numerical scheme for solving the mass balance equation, while the momentum and the energy equations are solved using the QUICK (Quadratic Upstream Interpolation for Convective Kinematics) scheme. Pressure–velocity coupling is achieved using the well-known SIMPLE algorithm. For the purpose of solution, the entire domain is divided into 17,345 nodes corresponding to 16,929 elements. A convergence criterion of maximum residual below  $10^{-8}$  is followed for determining convergence of the solution. The order of accuracy of all computed variables is ensured at least up to 4 significant digits after decimal point.

The solution of the aforementioned system of governing equations requires solving the energy balance equation for the solid phase of porous media as represented by Eq. (9). This is accomplished in ANSYS FLUENT by defining the solid-phase temperature ( $\theta_s$ ) as a user-defined scalar (UDS) (ANSYS 2012). The diffusive term in Eq. (9) is modelled using the DEFINE\_DIFFUSIVITY module of user-defined function. Heat transfer between the solid and the fluid phases as well as the internal heat generation in the solid phase is modelled as user-defined source terms using the DEFINE\_SOURCE module. All these functions are then coupled and solved using the UDS equation utility in ANSYS FLUENT. The individual components of the energy flux vector as well as all terms of entropy generation are also calculated by post-processing using user-defined functions.

### 4 Results and Discussion

The following results and discussion highlight the thermal non-equilibrium natural convective process in a cylindrical enclosure induced by heat generation in a truncated conical porous bed. Dimensions of the bed are maintained constant throughout the study at  $H' = 0.5$ ,  $R' = 0.25$  and  $\phi = 75^\circ$ . Water at 300 K (corresponding  $Pr$  of 5.83 and  $k_f = 0.610572$  W/m K) is assumed to fill the cylindrical enclosure and saturate the porous bed. Solid thermal conductivity is taken to be of the order of that found in nuclear debris beds or coal stockpiles ( $k_s = 2.0$  W/m K). Porosity ( $\epsilon$ ) of the porous bed is assumed to remain constant at 0.4. For the purpose of entropy generation analysis, height of the porous bed ( $H$ ) is assumed to be 0.5 m and the thermo-physical properties are calculated at the ambient temperature ( $T_c$ ) of 300 K. Effects of  $Ra$  and  $Da$  on fluid flow, heat transfer and entropy generation characteristics are sequentially discussed after reporting the grid independence and validation of the numerical model.

**Table 1** Grid Independence study using  $Nu_{avg}$  at the side wall (top row) and the top wall (bottom row) of the enclosure

$Ra$	$Da$	Configuration (number of nodes)		
		7802	17345	30650
$10^7$	$10^{-7}$	0.02289 (1.29%)	0.02314 (0.21%)	0.02319
		0.07807 (1.26%)	0.07895 (0.15%)	0.07907
		0.09671 (1.39%)	0.09789 (0.2%)	0.09808
$10^{11}$	$10^{-7}$	0.4341 (0.89%)	0.4376 (0.091%)	0.438

## 4.1 Grid Independence Study

In order to ensure that the solutions obtained are not influenced by the structure of computational domain, a grid independence study has been carried out with different configurations of the computational domain. Table 1 lists the  $Nu_{avg}$  values for both cold walls of the enclosure with three different configurations. It can be seen that as the grid is refined beyond 17,345 nodes, only a minor change takes place in  $Nu_{avg}$  for either cold wall of the enclosure. As such, this configuration has been utilised for performing further computations reported in the present work.

## 4.2 Validation of Numerical Results

Results obtained using the present numerical model are validated with the solution of Baytaş (2003) for a square enclosure with cold isothermal walls containing heat-generating porous media. Figure 2 presents a comparison between the present results and that of Baytaş (2003) in terms of  $Nu_{avg,s}$  and  $Nu_{avg,f}$  at the top wall for a wide range of  $h'$  and with  $\gamma = 1.0$ . In all cases,  $Ra$  and  $Da$  were kept constant at  $10^7$  and  $10^{-2}$ , respectively. The results show that the numerical solution closely matches the published results and as such, use of the numerical model for further study is well justified.

## 4.3 Fluid Flow and Heat Transfer Characteristics

In order to characterise the fluid flow and heat transfer patterns for the present problem, an analysis is carried out to determine the effects of volumetric heat generation (in terms of  $Ra$ ) and porous bed permeability (in terms of  $Da$ ). The effect of heat generation is investigated by performing a parametric study of  $Ra$  in the range of  $10^7$  to  $10^{11}$ , keeping  $Da$  fixed at  $10^{-7}$ . In a similar fashion, the effect of bed permeability is analysed by varying  $Da$  between  $10^{-6}$  and  $10^{-10}$  for a fixed  $Ra$  of  $10^{10}$ . Table 2 quantifies the pertinent global parameters for the range of study undertaken.

### 4.3.1 Effect of Rayleigh Number

The effect of  $Ra$  on fluid flow and heat transfer in the enclosure is represented in Fig. 3 with the help of streamlines, isotherms and energy flux vectors. Heat generation within the solid

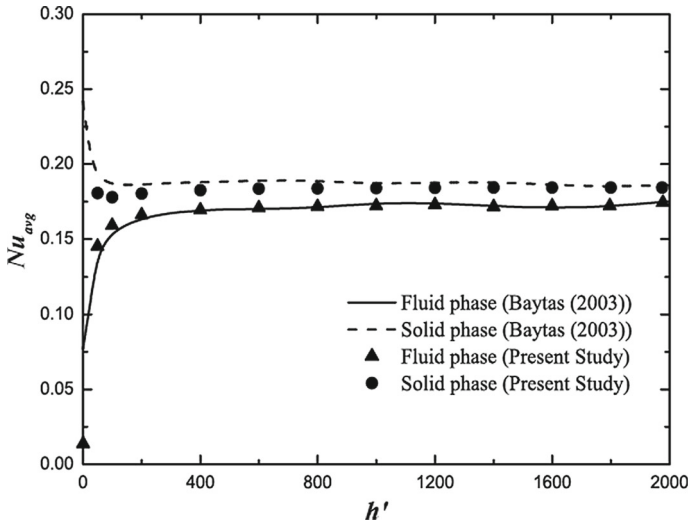


**Fig. 2** Comparison of the present numerical model with the solution of Baytas (2003) in terms of  $Nu_{avg}$  at the top wall for fluid and solid phases with  $Ra = 10^7$ ,  $Da = 10^{-2}$  and  $\gamma = 1.0$

**Table 2** Global parameters of the enclosure for the range of study undertaken in terms of  $Ra$  and  $Da$

$Ra$	$Da$	$RaDa$	$ \psi _{max}$	$\theta_{f,max}$	$\theta_{s,max}$	$Nu_{avg,side}$	$Nu_{avg,top}$
$10^7$	$10^{-7}$	1	7.9863	0.07804	0.08411	0.02314	0.07895
$10^8$		10	12.2602	0.07743	0.08348	0.030749	0.1023
$10^9$		$10^2$	21.6068	0.07597	0.08209	0.03874	0.12258
$10^{10}$		$10^3$	34.4527	0.0618	0.06938	0.05239	0.16529
$10^{11}$		$10^4$	51.914	0.03359	0.043796	0.097895	0.4376
$10^{10}$	$10^{-6}$	$10^4$	22.7519	0.02807	0.06069	0.060996	0.3223
	$10^{-7}$	$10^3$	34.4527	0.0618	0.06938	0.05239	0.16529
	$10^{-8}$	$10^2$	40.609	0.07915	0.08107	0.049	0.1426
	$10^{-9}$	10	41.7287	0.0812	0.0818	0.04904	0.13937
	$10^{-10}$	1	42.5094	0.08162	0.0818	0.04766	0.1314

phase of the porous bed results in heat transfer from the solid particles to the saturating fluid and induces a counter-clockwise natural convective circulation such that heat transfer takes place from the porous bed to the cold enclosure walls. Heat transfer also takes place from the heat-generating porous bed to the adjacent clear fluid region across the fluid–porous interface. The net heat transfer from the porous bed to the cold walls is, thus, a balance between these two competing heat transfer mechanisms. This is clearly depicted by the energy flux vectors in Fig. 3.

An increase in  $Ra$  is associated with a greater volumetric heat generation rate for a given bed geometry, which results in a higher  $\Delta T_{ref}$  and consequently induces stronger convection within the porous bed as well as the enclosure. This is evident from the gradually increasing trend of  $|\psi|_{max}$  with  $Ra$ , as shown in Table 2. Stronger convection leads to enhanced energy

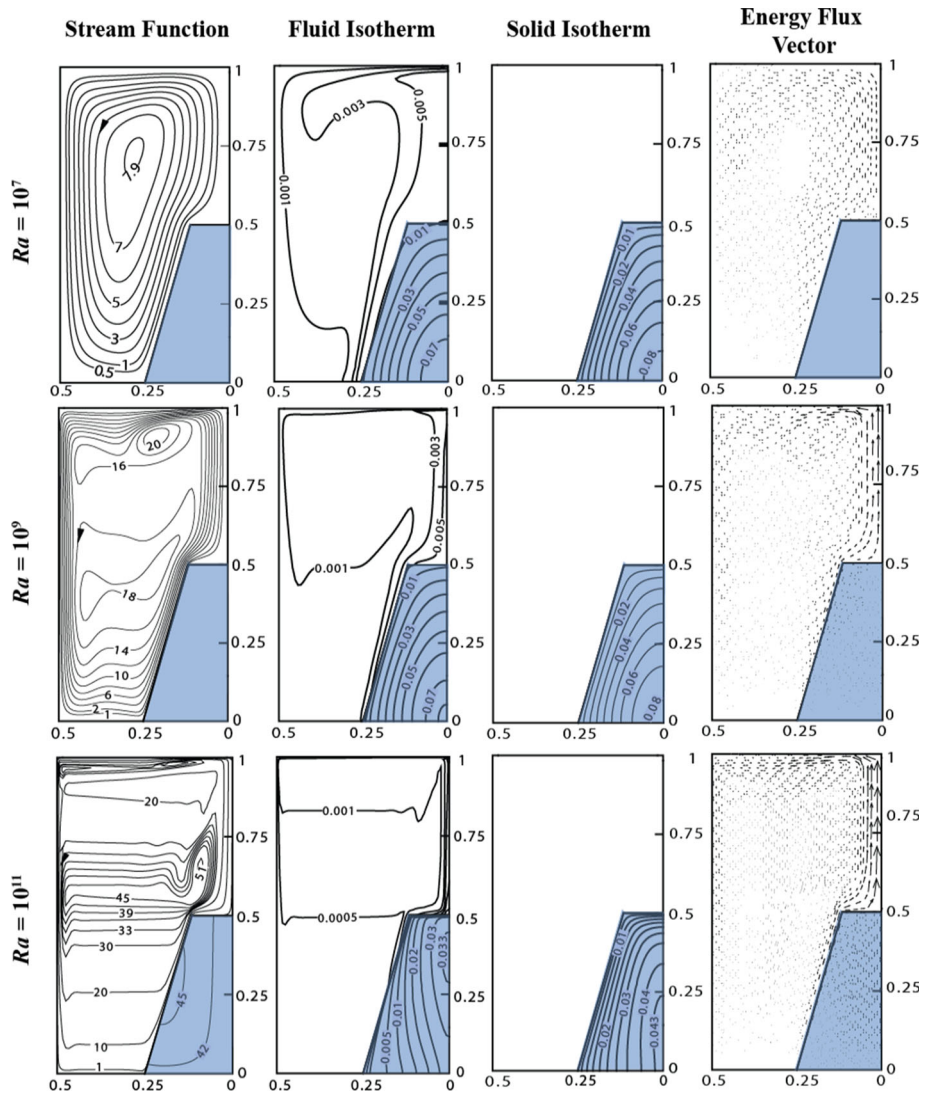


**Fig. 3** Stream function, isotherm and heat function contours for various  $Ra$  at  $Da = 10^{-7}$

transfer within the enclosure which in turn results in greater heat transfer at the cold walls. A visual observation of energy flux vectors for various  $Ra$  confirms the enhancement of energy transfer within the enclosure with increase in heat generation. The increase in heat transfer at the cold walls is evident from the magnitudes of  $Nu_{avg}$  in Table 2. Interestingly, both  $\theta_{s,max}$  and  $\theta_{f,max}$  have a decreasing trend with increase in  $Ra$  although greater heat generation in the porous bed must result in higher temperatures for both the phases. A review of the scaling parameters will show that the dimensionless temperature ( $\theta$ ) is determined by the relative values of temperature of the individual phases with respect to  $\Delta T_{ref}$ . Thus, although temperature of both phases is higher at higher  $Ra$ , the simultaneous increase in  $\Delta T_{ref}$  results in a reduced value of both  $\theta_{s,max}$  and  $\theta_{f,max}$ .

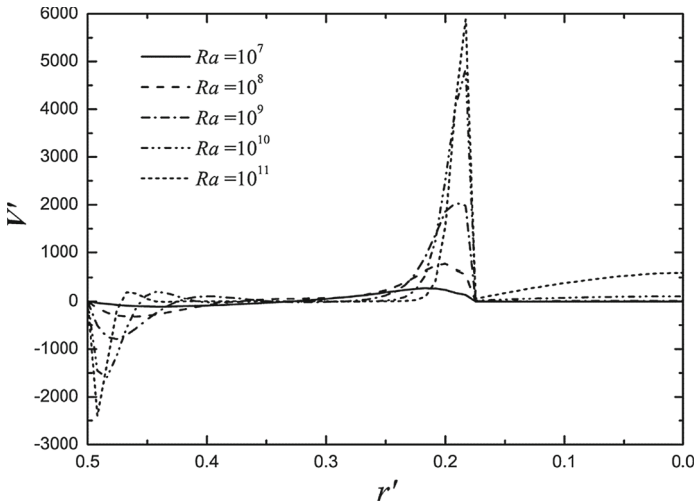


**Fig. 4** Dimensionless axial velocity profile along radial direction at  $z' = 0.25$  for various  $Ra$  at  $Da = 10^{-7}$

A comparison of energy flux vectors for different  $Ra$  in Fig. 3 reveals an interesting aspect of heat transfer mechanism from the porous bed. At lower heat generation rate (corresponding to  $Ra = 10^7$ ), heat transfer from the porous bed mainly takes place across the fluid–porous interface to the adjacent clear fluid region and subsequently, by convection to the cold walls. Heat transfer due to convection within the porous bed has a minor contribution to the overall heat transfer at such low heat generation. This lack of convection within the bed is also reflected by the overlapping solid and fluid isotherm in Fig. 3. With increase in heat generation (corresponding to  $Ra = 10^9$ ), however, the contribution of convective heat transfer within the porous bed increases and becomes comparable to heat transfer across the fluid–porous interface at still higher heat generation (corresponding to  $Ra = 10^{11}$ ). The corresponding fluid and solid isotherms in Fig. 3 also reflect this effect. Dimensionless axial velocity profiles along the radial direction in Fig. 4 at  $z' = 0.25$  (i.e. within the porous bed) further corroborate the above view.

Although greater heat transfer takes place at the cold walls at higher heat generation rates, i.e. at higher  $Ra$ , the variation in  $Nu_{avg}$  for either wall is not linear as can be seen from Fig. 5. The relative increase in heat transfer is higher at higher values of  $Ra$  for either wall. However, the increase in  $Nu_{avg}$  for the top wall is comparatively larger than that for the side wall. This is expected since natural convection drives the fluid within the porous bed in a counter-clockwise circulation such that maximum heat transfer takes place at the top wall and the residual energy is transferred to the side wall. This also accounts for the wide difference evident between the  $Nu_{avg}$  values of the top and side walls.

#### 4.3.2 Effect of Darcy Number

A change in Darcy number ( $Da$ ) essentially represents a modification of the fluid flow passage in the porous medium. Thus, a reduction in  $Da$  means greater resistance to fluid flow and hence, lower velocity and vice-versa. In the context of the present problem, a smaller value of  $Da$  for a certain  $Ra$  will reduce convection induced fluid motion within the porous bed. This is corroborated by the axial velocity profiles for various  $Da$  as shown in Fig. 6.

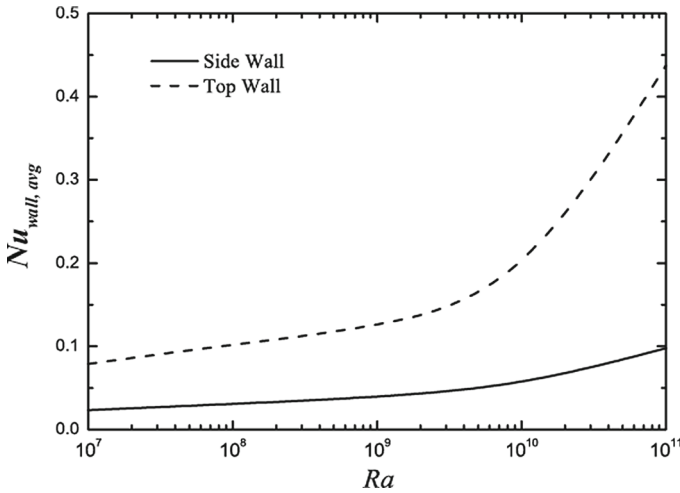


**Fig. 5** Variation of  $Nu_{avg}$  for top wall and side wall with  $Ra$  at  $Da = 10^{-7}$

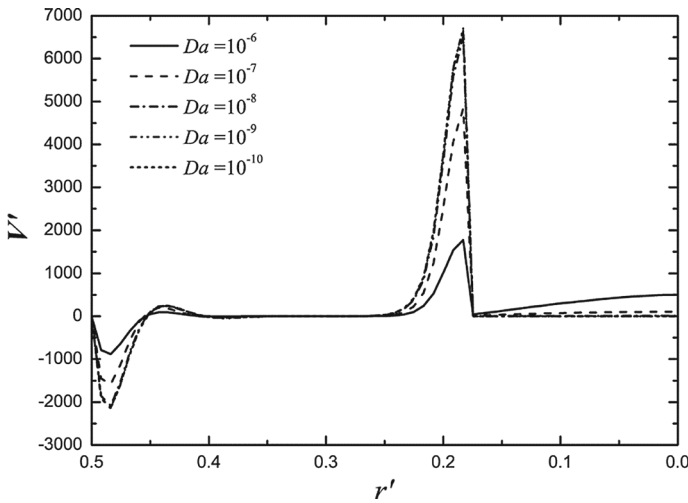


**Fig. 6** Dimensionless axial velocity profile along radial direction at  $z' = 0.25$  for various  $Da$  at  $Ra = 10^{10}$

A comparison of stream function, isotherm and energy flux vectors for three different  $Da$  ( $10^{-6}, 10^{-8}, 10^{-10}$ ) at  $Ra = 10^{10}$  is presented in Fig. 7. A high value of  $Da$ , i.e. greater bed permeability allows significant convective fluid motion to take place within the porous bed and hence, the dominant heat transfer mechanism from the bed is by convection of the saturating fluid. A decrease in bed permeability, as represented by reduction in  $Da$ , retards fluid motion within the bed and thereby leads to decreased contribution of convective heat transfer from the bed towards heat transfer in the enclosure. As a result, the enthalpy content of the porous bed increases and consequently the corresponding heat transfer across the fluid–porous interface also increases. A comparison of energy flux vectors in Fig. 8 adequately highlights this effect. Greater heat transfer leads to a higher fluid velocity along the interface, and thus successively greater velocity jumps are observed at the fluid–porous interface as  $Da$  is reduced in Fig. 6.



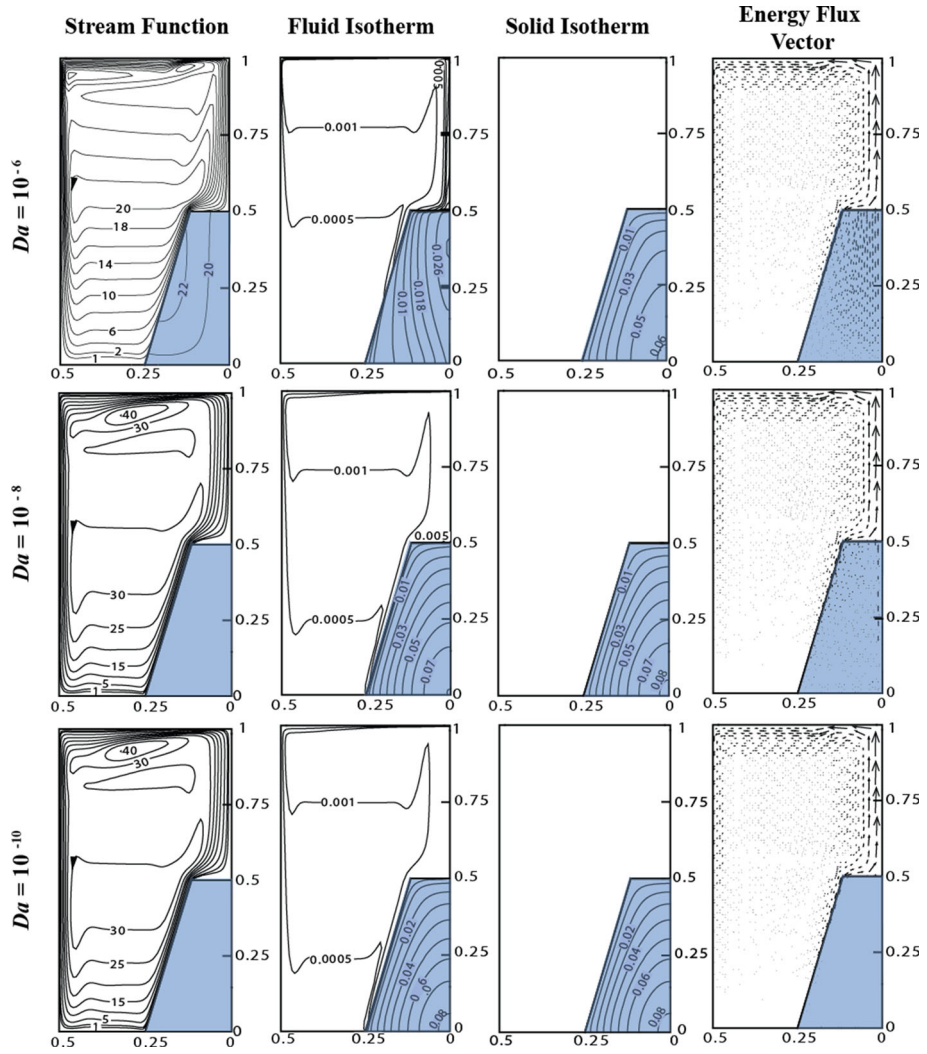


**Fig. 7** Stream function, isotherm and energy flux vectors for various  $Da$  at  $Ra = 10^{10}$

The net effect of reduced convective heat transfer from the bed is greater enthalpy content within the porous bed. As such, temperature rise within the bed is significantly higher at low  $Da$  as can be observed from the magnitude of  $\theta_{f,max}$  and  $\theta_{s,max}$  in Table 2. With the decrease in  $Da$  values, heat transfer from the bed and subsequently at the cold walls also decreases. This is represented in terms of  $Nu_{avg}$  at the cold walls for a given  $Ra$  in Fig. 8. It can be observed that the variation in  $Nu_{avg}$  with  $Da$  at a fixed  $Ra$  is similar to the variation of  $Nu_{avg}$  with  $Ra$  for a given  $Da$  in Fig. 5.

The above study on the effect of bed heat generation and bed permeability reveals some interesting aspects of natural convective flow in heat-generating porous media. Appreciable convection takes place within the porous bed for  $RaDa > 100$ , while it becomes negligible for  $RaDa < 100$ . As a consequence, convective heat transfer from the porous bed and heat transfer across the fluid–porous interface becomes the dominant heat transfer mechanism for

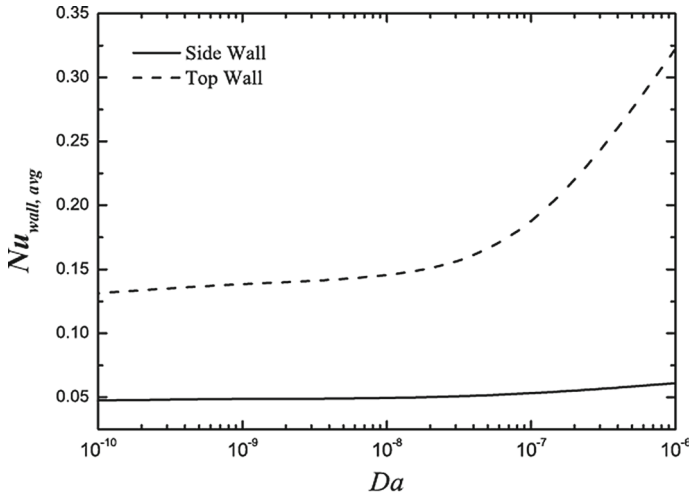


**Fig. 8** Variation of  $Nu_{avg}$  for top wall and side wall with  $Da$  at  $Ra = 10^{10}$

the two regimes, respectively. The dominance of convective heat transfer from the porous bed is also reflected by the rapid increase of  $Nu_{avg}$  beyond  $RaDa = 100$  in Figs. 5 and 8.

The above regime demarcation can also be used to identify problems with respect to the application of local thermal equilibrium (LTE) and local thermal non-equilibrium (LTNE) models of energy equation in porous media. It can be seen that for  $RaDa < 100$ , the magnitude of  $\theta_{s,max}$  tends to that of  $\theta_{f,max}$ , and the respective isotherms are almost overlapping. A significant difference, however, is evident at higher values of  $RaDa$ . Hence, it can be stated that the LTE model of energy equation may be applied to problems with  $RaDa < 100$  (i.e. conductive regime), while it must definitely not be used for problems involving  $RaDa > 100$  (i.e. convective regime).

#### 4.4 Entropy Generation Characteristics

The major objective of the entropy generation analysis presented in this section is to characterise the irreversibilities associated with natural convection, in an enclosure driven by heat-generating porous media. In order to have a comprehensive understanding, one representative case is presented here from each of the aforementioned heat transfer regimes. Figures 9 and 10 represent the local entropy generation contours pertaining to the cases with  $Ra = 10^8$ ,  $Da = 10^{-7}$  (i.e.  $RaDa < 100$ ) and  $Ra = 10^{10}$ ,  $Da = 10^{-7}$  ( $RaDa > 100$ ), respectively. This is followed by results of various factors contributing to entropy generation, as defined in Eqs. (27–31), with parametric variation in  $Ra$  and  $Da$ .

Observation reveals that entropy generation due to heat transfer irreversibility ( $NS''_{\theta}$ ) is concentrated near the cold walls of the enclosure and in the vicinity of the heat-generating porous bed, where the magnitude of temperature gradients is substantial. This can be seen from Figs. 9a and 10a. Since higher volumetric heat generation rate is associated with higher  $Ra$ , thermal gradients are also larger and consequently greater  $NS''_{\theta}$  is found at higher  $Ra$ .

Figures 9b and 10b represent the contours due to fluid friction irreversibility ( $NS''_{\psi}$ ). It can be seen that, in either case, maximum entropy generation takes place in the region above the porous bed and it progressively decreases in the counter-clockwise direction with minimum value in the porous bed. As the cold fluid picks up heat from the porous bed, its

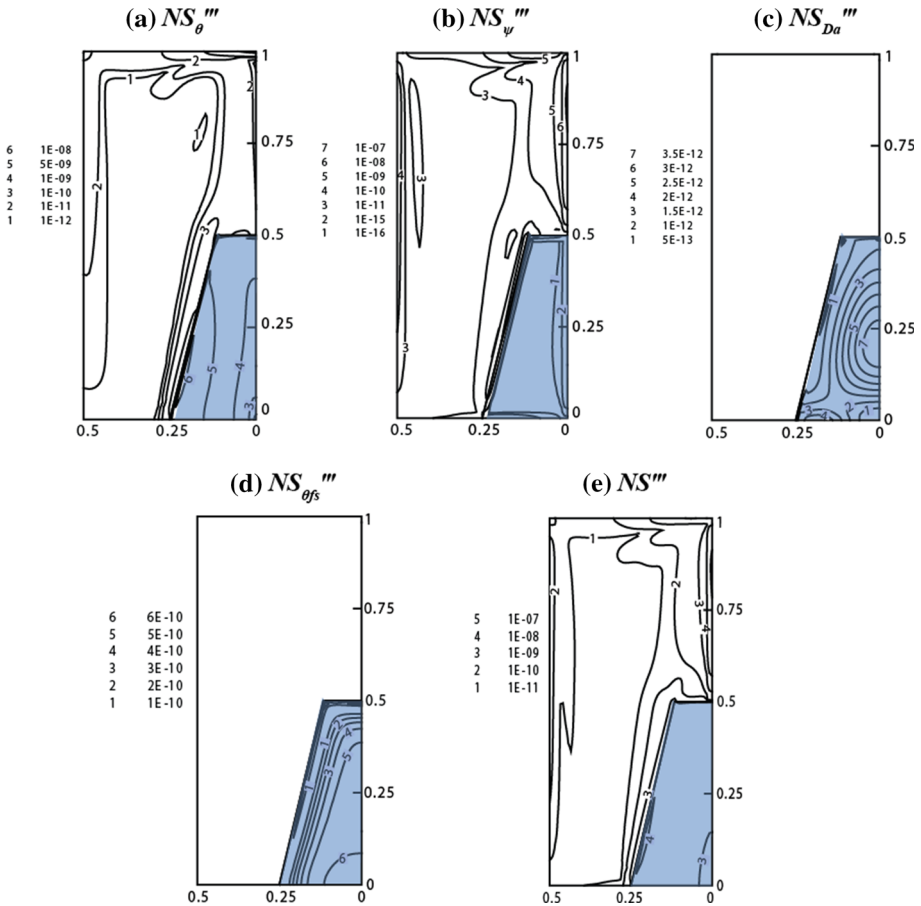
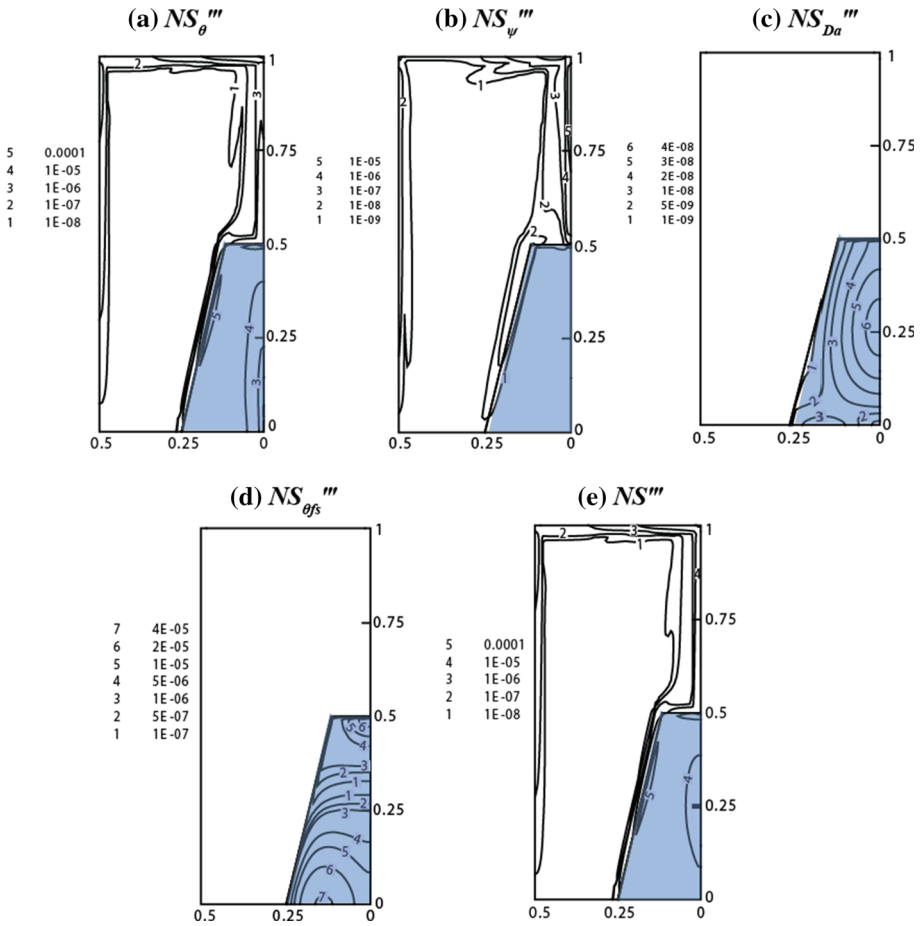


Fig. 9 Entropy generation contours at  $Ra = 10^8$ ,  $Da = 10^{-7}$

velocity rapidly increases and attains maximum magnitude above the porous bed. As such, fluid friction irreversibility is also greater in this region. The heated fluid deposits energy first at the top wall and then at the side wall, and its velocity gradually decreases with a corresponding decrease in entropy generation. Flow resistance within the porous bed results in a very low velocity in this region, and consequently entropy generation is also minimum in the porous bed. Similar to the case of heat transfer irreversibility, higher  $Ra$  induces a larger fluid velocity and thereby  $NS_{\psi}'''$  is also greater at higher  $Ra$ .

The contours of entropy generation due to viscous drag ( $NS_{Da}'''$ ) in the porous bed are shown in Figs. 9c and 10c. Only a minor variation is observed in the magnitude of the contours for both the cases, with greater entropy generation in inner regions of the porous bed. This happens since flow velocity marginally increases towards the inner regions of the bed, as can be seen from Fig. 4. As expected,  $NS_{Da}'''$  also has a greater magnitude at higher  $Ra$  since larger volumetric heat generation induces stronger flow in the porous bed.

Entropy generation contours due to solid to fluid heat transfer in the porous bed ( $NS_{\theta fs}'''$ ) are represented in Figs. 9d and 10d. In the regime with  $Ra = 10^8$  and  $Da = 10^{-7}$ , i.e.  $RaDa < 100$ , a lack of convective heat transfer from the porous bed results in the establishment of an



**Fig. 10** Entropy generation contours at  $Ra = 10^{10}$ ,  $Da = 10^{-7}$

almost uniform temperature gradient within the bed for either phase of the porous medium. As such,  $NS''''_{\theta fs}$  is also uniform with progressively greater magnitude towards the inner region due to a marginally higher temperature gradient. This is depicted in Fig. 9d. The effect of greater convection within the porous bed at higher  $Ra$  is evident from the contour in Fig. 10d.

The global magnitudes of various entropy generation terms for parametric variations in  $Ra$  and  $Da$  are listed in Table 3. The range of  $Ra$  and  $Da$  chosen for this analysis is kept similar to that in fluid flow and heat transfer analysis (Sect. 4.3) for enabling better interpretation of the results. The dominant mechanism for entropy generation can easily be identified using Bejan number ( $Be$ ) as defined in Eq. (34). It is worth mentioning here that  $Be > 0.5$  represents dominancy of heat transfer irreversibility, while  $Be < 0.5$  indicates that fluid friction irreversibility is the dominant mechanism. A significant variation in  $Be$  is observed as  $Ra$  is varied at a constant  $Da$ . Only minor variations are, however, observed in case of variations in  $Da$  at a constant  $Ra$ .

At low heat generation rates (i.e. low  $Ra$ ), lower temperature rise of solid particles results in negligible solid to fluid heat transfer in the porous region and thereby, thermal gradients for both solid and fluid phases are weak. As such, the contribution of entropy generation

**Table 3** Global entropy generation parameters of the enclosure for the range of study undertaken in terms of  $Ra$  and  $Da$

$Ra$	$Da$	$RaDa$	$NS''_{\theta}$	$NS''_{\psi}$	$NS''_{Da}$	$NS''_{\theta fs}$	$NS''$	$Be$
$10^7$	$10^{-7}$	1	$5.51 \times 10^{-8}$	$3.29 \times 10^{-7}$	$2.37 \times 10^{-11}$	$5.43 \times 10^{-9}$	$3.9 \times 10^{-7}$	0.1552
$10^8$		10	$5.66 \times 10^{-6}$	$4.89 \times 10^{-6}$	$2.22 \times 10^{-9}$	$5.33 \times 10^{-7}$	$1.11 \times 10^{-5}$	0.5586
$10^9$		$10^2$	0.00058	$5.31 \times 10^{-5}$	$2.24 \times 10^{-7}$	$5.06 \times 10^{-5}$	$6.84 \times 10^{-4}$	0.9221
$10^{10}$		$10^3$	0.05947	0.00076	$2.42 \times 10^{-5}$	0.01188	$7.21 \times 10^{-2}$	0.9892
$10^{11}$		$10^4$	4.80866	0.01856	0.00085	3.52924	8.3573	0.9977
$10^{10}$	$10^{-6}$	$10^4$	0.05043	0.00211	$5.70 \times 10^{-5}$	0.05575	$1.09 \times 10^{-1}$	0.9754
	$10^{-7}$	$10^3$	0.05947	0.00076	$2.42 \times 10^{-5}$	0.01188	$7.21 \times 10^{-2}$	0.9892
	$10^{-8}$	$10^2$	0.06066	0.00041	$2.46 \times 10^{-6}$	0.00199	$6.31 \times 10^{-2}$	0.9934
	$10^{-9}$	10	0.06112	0.00036	$2.50 \times 10^{-7}$	0.000804	$6.23 \times 10^{-2}$	0.9941
	$10^{-10}$	1	0.06138	0.00032	$2.52 \times 10^{-8}$	0.000322	$6.20 \times 10^{-2}$	0.9948

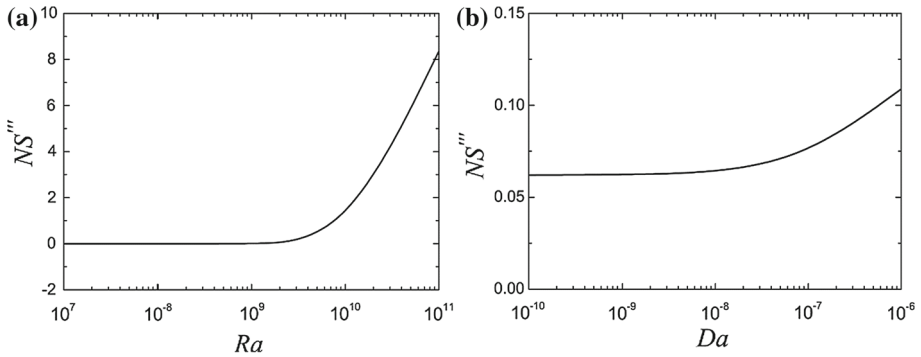


**Fig. 11** Variation of Total Entropy generation ( $NS'''$ ) with a  $Ra$  at  $Da = 10^{-7}$  and b  $Da$  at  $Ra = 10^{10}$

due to heat transfer irreversibility (combined contribution of  $NS'''_{\theta}$  and  $NS'''_{\theta fs}$ ) towards total entropy generation is small as compared to that from fluid friction irreversibility ( $NS'''_{\psi}$ ). This is reflected by a small magnitude of  $Be$  (corresponding to  $Ra = 10^7$ ). An increase in the volumetric heat generation rate (i.e. increase in  $Ra$ ) leads to a higher solid-phase temperature in the porous bed. This necessitates a greater solid–fluid heat transfer within the porous bed and consequently establishes a stronger thermal gradient for both phase of the porous medium. As such, the magnitude of heat transfer irreversibility within the porous bed becomes higher as  $Ra$  is increased. Heat transfer irreversibility in the clear fluid region is also higher since greater energy transfer from the porous bed results in larger heat transfer at the cold enclosure walls. As such, the overall entropy generation due to heat transfer irreversibility becomes higher as  $Ra$  is increased. This increase in energy transfer also leads to stronger convection within the porous bed as well as the clear fluid region. Therefore, irreversibilities associated with fluid friction and viscous drag in porous bed also increase simultaneously. Interestingly, the least contribution to entropy generation for the entire range of  $Ra$  comes from viscous drag within the porous bed ( $NS'''_{Da}$ ) due to small flow velocities in the region. A comparison of  $Be$  reveals that irreversibilities due to heat transfer and other sources become almost comparable to each other at  $Ra = 10^8$ , while increasing  $Ra$  beyond results in significantly greater dominancy of heat transfer irreversibility.

In case of variations in  $Da$  keeping  $Ra$  fixed, all entropy generation terms except  $NS'''_{\theta}$  exhibit an increasing nature with increase in  $Da$ . An increase in  $Da$  allows greater fluid flow in porous media leading to higher fluid velocities in the porous bed as well as in the clear fluid region. As such, irreversibility related to both fluid friction ( $NS'''_{\psi}$ ) as well as viscous drag in the porous bed ( $NS'''_{Da}$ ) is of a greater magnitude at higher  $Da$ . For the same heat generation rate (since  $Ra$  is constant) at higher  $Da$ , a stronger flow leads to greater convective energy transfer from the porous bed and as such, results in a weaker thermal gradient within the porous bed (as is evident from Fig. 7). At the same time, a stronger convective energy transfer establishes a marginally greater thermal gradient near the cold enclosure walls at higher  $Da$  and thereby causes greater heat transfer at the cold walls (as represented in Fig. 8). However, observation reveals that the relative change in thermal gradient is much larger within the porous bed than near the cold walls. Thus,  $NS'''_{\theta}$  is governed by thermal gradients within the porous bed such that it decreases with an increase in  $Da$ . Further, greater convection within the porous bed with increase in  $Da$  results in a larger temperature difference between the solid and fluid phases (as can be seen from Table 2 as well as isotherms in Fig. 7) and hence  $NS'''_{\theta fs}$  also increase with  $Da$ . However, no significant change is observed in  $Be$  with  $Da$  signifying that the dominant mode of entropy generation is independent of  $Da$ .

Figure 11 represents the variation of  $NS'$  with  $Ra$  and  $Da$ , respectively. Interestingly, the variations are similar to that of  $Nu_{avg}$  in Figs. 6 and 9 justifying the assumption that entropy generation within the enclosure can also be demarcated into the aforementioned heat transfer regimes at a critical  $RaDa$  of 100.

## 5 Summary and Conclusions

The steady-state flow, heat transfer and entropy generation characteristics have been numerically investigated for a two-dimensional, laminar natural convective flow in a cylindrical enclosure induced by a heat-generating porous bed. Darcy–Brinkmann–Forchheimer model and local thermal non-equilibrium (LTNE) have been adopted for describing momentum and energy transport in porous medium, respectively. Analysis has been carried out for a wide range of  $Ra$  ( $10^7$ – $10^{11}$ ) and  $Da$  ( $10^{-6}$ – $10^{-10}$ ) with  $Pr = 5.83$  and  $\varepsilon = 0.4$ . Some salient observations from the study are summarised as follows

1. Fluid flow and heat transfer within the enclosure are mainly governed by the relative magnitudes of  $Ra$  and  $Da$ . Although heat transfer in the clear fluid region is always convection-dominated, two distinct heat transfer regimes have been identified within the porous bed at critical  $RaDa$  of 100—heat transfer from porous region takes place mainly to the adjacent fluid region across the fluid–porous interface when  $RaDa < 100$  and by convection of the saturating fluid when  $RaDa > 100$ .
2. Significantly greater heat transfer is observed at the cold enclosure walls in the convection-dominated regime.
3. The case of local thermal equilibrium (LTE) has been recovered for cases in the conduction-dominated regime, while it is observed that local thermal non-equilibrium (LTNE) must be adopted for cases in the convection-dominated regime.
4. The least contribution to entropy generation within the enclosure is from  $NS'''_{Da}$  irrespective of heat transfer regime.
5. Major contribution to entropy generation comes from  $NS''_{\psi}$  for low heat generation rates (i.e. low  $Ra$ ), while at higher heat generation rates the contribution from  $NS''_{\theta}$  and  $NS''_{\theta fs}$  exceeds that of other factors.

**Acknowledgements** The authors are grateful to AREVA for providing AREVA PhD fellowship to the first author, and to the Department of Science and Technology (DST), Government of India for providing fellowship to the second author under the INSPIRE programme. The authors would also like to thank Dr. Pallab Sinha Mahapatra, Postdoctoral fellow, University of Illinois at Chicago, for helping out in the review process.

## References

- Alazmi, B., Vafai, K.: Analysis of variants within the porous media transport models. *J. Heat Transf.* **122**, 303–326 (2000)
- Alazmi, B., Vafai, K.: Constant wall heat flux boundary conditions in porous media under local thermal non-equilibrium conditions. *Int. J. Heat Mass Transf.* **45**, 3071–3087 (2002)
- ANSYS Inc.: ANSYS Fluent UDF Manual Release 14.5 (2012)
- Baytaş, A.C.: Thermal non-equilibrium natural convection in a square enclosure filled with a heat-generating solid phase, non-Darcy porous medium. *Int. J. Energy Res.* **27**, 975–988 (2003)
- Baytaş, A.C.: Entropy generation for thermal nonequilibrium natural convection with a non-darcy flow model in a porous enclosure filled with a heat-generating solid phase. *J. Porous Media* **10**, 261–275 (2007)
- Baytaş, A.C., Pop, I.: Free convection in a square porous cavity using a thermal nonequilibrium model. *Int. J. Therm. Sci.* **41**, 861–870 (2002)

- Bejan, A.: Entropy generation minimization: the new thermodynamics of finite-size devices and finite-time processes. *J. Appl. Phys.* **79**, 1191–1218 (1996)
- Betchen, L.J., Straatman, A.G.: The development of a volume-averaged entropy-generation function for non-equilibrium heat transfer in high conductivity porous foams. *Numer. Heat Transf. Part B. Fund.* **53**, 412–436 (2008)
- Bortolozzi, R.A., Deiber, J.A.: Comparison between two- and one-field models for natural convection in porous media. *Chem. Eng. Sci.* **56**, 157–172 (2001)
- Chakravarty, A., Datta, P., Ghosh, K., Sen, S., Mukhopadhyay, A.: Numerical analysis of a heat-generating, truncated conical porous bed in a fluid-filled enclosure. *Energy* **106**, 646–661 (2016)
- Chen, Y.H., Lin, H.T.: Natural convection in an inclined enclosure with a fluid layer and a heat-generating porous bed. *Heat Mass Transf.* **33**, 247–255 (1997)
- Datta, P., Mahapatra, P.S., Ghosh, K., Manna, N.K., Sen, S.: Heat transfer and entropy generation in a porous square enclosure in presence of an adiabatic block. *Transp. Porous Media* **111**, 105–129 (2016)
- Dixon, A.G., Cresswell, D.L.: Theoretical prediction of effective heat transfer parameters in packed beds. *AIChE J.* **25**, 663–676 (1979)
- Du, Z.G., Bilgen, E.: Natural convection in vertical cavities with partially filled heat-generating porous media. *Numer. Heat Transf. Part A Appl.* **18**, 371–386 (1990)
- Ejlali, A., Ejlali, A., Hooman, K., Gurgenci, H.: Application of high porosity metal foams as air-cooled heat exchangers to high heat load removal systems. *Int. Commun. Heat Mass Transf.* **36**, 674–679 (2009)
- Ejlali, A., Hooman, K.: Buoyancy effects on cooling a heat generating porous medium: Coal Stockpile. *Transp. Porous Media* **88**, 235–248 (2011)
- Faghri, A., Zhang, Y.: *Transport Phenomena in Multiphase Systems*. Elsevier, Amsterdam (2006)
- Famouri, M., Hooman, K.: Entropy generation for natural convection by heated partitions in a cavity. *Int. Commun. Heat Mass Transf.* **35**, 492–502 (2008)
- Glassley, W.E.: *Geothermal Energy: Renewable Energy and the Environment*, 2nd edn. CRC Press, Taylor & Francis Group, London (1995)
- Hooman, K.: Energy flux vectors as a new tool for convective visualisation. *Int. J. Numer. Methods Heat Fluid Flow* **20**, 240–249 (2010)
- Jue, T.C.: Analysis of thermal convection in a fluid-saturated porous cavity with internal heat generation. *Heat Mass Transf.* **40**, 83–89 (2003)
- Kakaç, S., Kilkış, B., Kulacki, F.A., Arinç, F.: *Convective heat and mass transfer in porous media*, 1st edn. Springer, Çeşme, Turkey (1991)
- Kaluri, R.S., Basak, T.: Entropy generation due to natural convection in discretely heated porous square cavities. *Energy* **36**, 5065–5080 (2011)
- Kim, G.B., Hyun, J.M., Kwak, H.S.: Buoyant convection in a square cavity partially filled with a heat-generating porous medium. *Numer. Heat Transf. Part A Appl.* **40**(6), 601–618 (2001)
- Kimura, S., Bejan, A.: The “heatline” visualization of convective heat transfer. *J. Heat Transf.* **105**, 916–919 (1983)
- Kuznetsov, A.V., Nield, D.A.: Local thermal non-equilibrium and heterogeneity effects on the onset of convection in an internally heated porous medium. *Transp. Porous Media* **102**, 15–30 (2014)
- Kuznetsov, A.V., Nield, D.A.: Local thermal non-equilibrium effects on the onset of convection in an internally heated layered porous medium with vertical throughflow. *Int. J. Therm. Sci.* **92**, 97–105 (2015)
- Mahapatra, P.S., Manna, N.K., Ghosh, K.: Hydrodynamic and thermal interactions of a cluster of solid particles in a pool of liquid of different Prandtl numbers using two-fluid model. *Heat Mass Transf.* **49**, 1659–1679 (2013)
- Mahmoudi, Y.: Constant wall heat flux boundary condition in micro-channels filled with a porous medium with internal heat generation under local thermal non-equilibrium condition. *Int. J. Heat Mass Transf.* **85**, 524–542 (2015)
- Mckenzie, D.P., Roberts, J.M., Weiss, N.O.: Convection in the earth’s mantle: toward a numerical simulation. *J. Fluid Mech.* **62**, 465–538 (1974)
- Minkowycz, W.J., Haji-Sheikh, A., Vafai, K.: On departure from local thermal equilibrium in porous media due to a rapidly changing heat source: The Sparrow number. *Int. J. Heat Mass Transf.* **42**, 3373–3385 (1999)
- Mukhopadhyay, A.: Analysis of entropy generation due to natural convection in square enclosures with multiple discrete heat sources. *Int. Commun. Heat Mass Transf.* **37**, 867–872 (2010)
- Nield, D., Bejan, A.: *Convection in Porous Media*, 3rd edn. Springer, New York (2006)
- Nield, D.A., Kuznetsov, A.V., Xiong, M.: Effect of local thermal non-equilibrium on thermally developing forced convection in a porous medium. *Int. J. Heat Mass Transf.* **45**, 4949–4955 (2002)
- Nouri-Borujerdi, A., Noghrehabadi, A.R., Rees, D.A.S.: The effect of local thermal non-equilibrium on conduction in porous channels with a uniform heat source. *Transp. Porous Media* **69**, 281–288 (2007a)



- Nouri-Borujerdi, A., Noghrehabadi, A.R., Rees, D.A.S.: Onset of convection in a horizontal porous channel with uniform heat generation using a thermal nonequilibrium model. *Transp. Porous Media* **69**, 343–357 (2007b)
- Prasad, V.: Thermal convection in a rectangular cavity filled with heat-generating, Darcy porous medium. *J. Heat Transf.* **109**, 697–703 (1987)
- Ranz, W.E., Marshall, W.M.: Evaporation from Drops. *Chem. Eng. Prog.* **48**, 141–146 (1952)
- Rees, D.A.S., Pop, I.: Local thermal non-equilibrium in porous medium convection. In: Ingham, D.B., Pop, I. (eds.) *Transport Phenomena in Porous Media*, vol. III, pp. 147–174. Elsevier, Oxford (2005)
- Saravanan, S.: Thermal non-equilibrium porous convection with heat generation and density maximum. *Transp. Porous Media* **76**, 35–43 (2009)
- Saravanan, S., SenthilNayagi, V.P.M.: Thermorheological effect on thermal nonequilibrium porous convection with heat generation. *Int. J. Eng. Sci.* **74**, 55–64 (2014)
- Schulenberg, T., Muller, U.: Natural convection in saturated porous layers with internal heat sources. *Int. J. Heat Mass Transf.* **27**(5), 677–685 (1984)
- Takasuo, E.: Coolability of porous core debris beds: Effects of bed geometry and multi-dimensional flooding. VTT Technical Research Centre of Finland (2015)
- Takasuo, E., Holmström, S., Kinnunen, T., Pankakoski, P.: The COOLOCE experiments investigating the dryout power in debris beds of heap-like and cylindrical geometries. *Nucl. Eng. Des.* **250**, 687–700 (2012)
- Ting, T.W., Hung, Y.M., Guo, N.: Entropy generation of viscous dissipative nanofluid flow in thermal non-equilibrium porous media embedded in microchannels. *Int. J. Heat Mass Transf.* **81**, 862–877 (2015)
- Torabi, M., Karimi, N., Zhang, K.: Heat transfer and second law analyses of forced convection in a channel partially filled by porous media and featuring internal heat sources. *Energy* **93**, 106–127 (2015a)
- Torabi, M., Zhang, K., Yang, G., Wang, J., Wu, P.: Heat transfer and entropy generation analyses in a channel partially filled with porous media using local thermal non-equilibrium model. *Energy* **82**, 922–938 (2015b)
- Toth, F.L.: *Geological Disposal of Carbon Dioxide and Radioactive Waste: A Comparative Assessment*. Springer, New York (2011)
- Wakao, N., Kaguei, S., Funazkri, T.: Effect of fluid dispersion coefficients on particle-to-fluid heat transfer coefficients in packed beds. *Chem. Eng. Sci.* **34**, 326–336 (1979)
- Wu, F., Wang, G., Zhou, W.: A thermal nonequilibrium approach to natural convection in a square enclosure due to the partially cooled sidewalls of the enclosure. *Numer. Heat Transf. Part A Appl.* **67**, 771–790 (2015a)
- Wu, F., Zhou, W., Ma, X.: Natural convection in a porous rectangular enclosure with sinusoidal temperature distributions on both side walls using a thermal non-equilibrium model. *Int. J. Heat Mass Transf.* **85**, 756–771 (2015b)